Single cell sequencing reveals heterogenicity of differential gene expression and altered interactome in post-ischemic mouse brain cells

Ting Lu[1], Shengzhen Hou[2], Liyun Wang[3], Haitao Li[2], Zunlu Zhang[2], Mingzhe Hu[2], Jinping Zhang[2]

[1]Department of Neurology, The First Affiliated Hospital of Shandong First Medical University, Jinan City, Shandong Province, 250014, China
[2]Department of Neurology, Affiliated Hospital of Shandong University of Traditional Chinese Medicine, Jinan City, Shandong Province, 250014, China
[3]Department of Gastroenterology, The First Affiliated Hospital of Shandong First Medical University, Jinan City, Shandong Province, 250014, China

Submitted: 5 March 2024; **Accepted:** 14 June 2024
Online publication: 21 June 2024

Arch Med Sci
DOI: https://doi.org/10.5114/aoms/190069

Corresponding author:
Jinping Zhang, MD, PhD
Department of Neurology
Affiliated Hospital
of Shandong University
of Traditional Chinese Medicine
No. 16369#, Jingshi Road
Jinan City
Shandong Province, 250014,
China
E-mail: zhangjinpingdoctor@126.com

Abstract

Introduction: Ischemia, resulting from reduced blood supply, poses a critical health challenge. It is known to be caused by arterial constriction or blockages and triggers oxygen and nutrient deprivation, impacting multiple body systems and leading to a multitude of diseases and associated health conditions. Due to its multifaceted association with several diseases, ischemia is a subject of interest in many clinical studies. Over several decades of information on ischemia and related molecular changes have provided valuable insight into its pathophysiological outcomes. However, the scarcity of molecular studies, especially genomic inquiries employing spatial and temporal segregation, remains mostly unaddressed. The emerging field of single-cell genomics offers promising solutions to such inquiries. Therefore, we performed our study by utilizing a single-cell genomics approach, employing a mouse brain model of hypoxia at two distinct time points (30 min and 60 min of exposure with hypoxia) to delineate cellular trajectories, ontology, and the clustering of expression-based patterns in a cell-specific manner.

Material and methods: In the present study we developed a mouse model of hypoxia, which was established using the thread-plug method. The experimental groups were subjected to hypoxia for 30 min (T_30) and 60 min (T_60), while the sham surgery group was used as a control. Following excision of the cerebral cortex, nuclear isolation and library construction were performed before conducting spatio-temporal analysis of cortical cells. Comprehensive data analysis encompassed differential gene expression analysis, trajectory analysis, examination of gene regulatory networks, and hallmark analysis.

Results: The primary outcome of the single cell genomics analysis emerged as clustering of 12 distinct cell populations suggesting contrasting transcriptomic profiles. Furthermore, spatio-temporal distinction in cell signaling was identified as a switch from Ras GTPase signaling to calmodulin and calcium dependent signaling between two levels of ischemia. The most dynamic regions in terms of transcription were distal axons and growth cones in the T_30 group, and cell edges and the post-synaptic area in the T_60 group. Also, the synaptic vesicle cycle is likely to be involved in such transcription switching.

Conclusions: Our study employing a single-cell genomics approach provides valuable insights into the cellular dynamics during hypoxia exposure. The identified cell populations and associated molecular pathways offer potential targets for further research and development of targeted therapies in addressing the complex challenges posed by ischemia.

Key words: hypoxia, cerebral ischemia, single cell genomics, neuronal cells, Hif-1.

Introduction

Ischemia, characterized by reduced blood supply to tissues, significantly impacts human health by depriving organs of oxygen and essential nutrients [1, 2]. This condition can lead to serious physiological issues, including strokes, which may include subarachnoid hemorrhage, intracerebral hemorrhage, and ischemic stroke [3]. Ischemic strokes, marked by sudden or waking neurologic deficits, constitute about 80% of strokes and account for 11% of global deaths according to the World Health Organization [4]. Cerebrovascular diseases rank as the second leading cause of mortality and dementia worldwide, and the third leading cause of death among men. Stroke incidence varies globally, averaging 200 cases per 100,000 inhabitants, with higher rates in non-industrialized nations [5, 6]. Japan has the highest stroke incidence, while the UK, Germany, and New Zealand report the lowest. Incidence increases with age, particularly in individuals over 55 years, with higher rates in Japan, Russia, and Ukraine. Males consistently show a higher incidence than females, and China has the highest estimated lifetime risk of stroke [7]. A 2013 survey in China reported an age-standardized prevalence, incidence, and mortality of stroke of 1.1%, 246.8 per 100,000 person-years, and 114.8 per 100,000 person-years, respectively [8]. Stroke incidence follows a circadian rhythm, peaking between 6 am and 12 noon, with 55% of ischemic strokes occurring during this period [9]. Ischemic stroke typically presents with dysarthria and unilateral weakness, but can be mimicked by seizures, conversion disorders, migraines, and hypoglycemia [10]. Post-stroke conditions can range from lethality to significant disabilities, such as paralysis, speech issues, and cognitive impairments, posing severe challenges to individuals [11]. Preventive strategies for ischemic stroke involve improving care systems to minimize treatment delays and swiftly administering reperfusion therapies such as intravenous thrombolysis, which significantly reduce disability if given within 4.5 h of onset [12]. Thrombolysis can be extended up to 9 h after onset for patients with salvageable brain tissue, and endovascular thrombectomy is highly effective within 6 h of onset for large vessel occlusions [13]. Selected patients, identified through perfusion imaging, may benefit from thrombectomy up to 24 h after onset, further reducing disability. Post-stroke management focuses on secondary prevention, including blood pressure control, cholesterol management, and appropriate antithrombotic medications to prevent recurrent strokes [14, 15]. Tailored interventions, such as anticoagulation for atrial fibrillation and carotid endarterectomy for severe symptomatic carotid artery stenosis, are crucial. These measures aim to reduce the incidence and impact of ischemic strokes, enhancing patient outcomes and minimizing long-term disability [16].

The cerebrum, a key brain region governing motor function, vision, hearing, and analytical reasoning, promptly responds to ischemia [17]. Ischemic stroke triggers a cascade of molecular events in the cerebrum, leading to significant neuronal damage and subsequent functional impairments. Researchers have investigated neuroprotection, regeneration processes, and associated molecular pathways to mitigate this damage. Ischemia-induced vascular obstruction generates excessive reactive oxygen species (ROS), intensifying neuronal injury through oxidative stress. Identifying pathways that respond to and mitigate oxidative stress is critical for minimizing injuries. Moreover, ischemia-induced inflammation exacerbates post-stroke neuronal damage, highlighting the importance of effectively modulating immune responses to reduce injuries. Animal models, such as middle cerebral artery occlusion (MCAO) in murine models, offer valuable insights into stroke mechanisms and simulate clinical interventions such as mechanical thrombolysis, providing insights into potential future treatments. Despite extensive research and the availability of high-throughput data, significant gaps persist in understanding the intricate genomics and transcriptomics underlying ischemic stroke. Comprehensive elucidation of genomic factors contributing to an individual's susceptibility, such as specific genetic variants or mutations predisposing individuals to vascular pathology, remains incomplete. Additionally, understanding transcriptomic alterations within various brain cell types, particularly their variable spatio-temporal response to ischemic insults and their implications in disease progression, is an area with limited comprehension. Single-cell sequencing emerges as a promising avenue to address these knowledge gaps. Traditional bulk sequencing methods often mask the inherent heterogeneity in complex tissues such as the brain. Single-cell sequencing technologies allow researchers to explore the intricacies of individual cells, revealing cell-specific genetic and transcriptomic signatures in response to an ischemic insult. This approach facilitates the identification of rare cell populations crucial in cerebral ischemia pathophysiology, often overlooked in bulk analyses. By employing single-cell sequencing techniques, it is possible to unravel the heterogeneity of brain cell types affected by ischemia. This includes identifying distinct molecular profiles associated with different neuronal subtypes, glial cells, endothelial cells, and immune cells. The method also aids in exploring temporal changes in gene expression during various stages of ischemic injury, shedding light on dynamic molecular responses within specific cell populations. Moreover,

single-cell sequencing can help identify previously unrecognized genetic variants or transcriptomic alterations specific to certain vulnerable or resilient cell types in response to an ischemic insult. Deciphering these molecular signatures at the single-cell level holds the potential to pinpoint novel therapeutic targets or pathways for intervention, enabling the development of more tailored treatments to mitigate the impact of cerebral ischemia. Therefore, single-cell sequencing was used to achieve the primary objective of the study, which was mainly to look at the cellular heterogenicity in terms of the response to a hypoxic insult, which is otherwise not possible in conventional approaches. Hence the use of a single-cell approach (which itself is a state-of-the-art technology, although with some limitations) was explored as a potential means to update the knowledge and understanding of ischemia-induced changes. In the present study, we conducted single-cell transcriptomic analysis on the mice's cerebral cortex, subjecting it to two distinct ischemia regimens over a temporal scale of 30 min and 60 min. These conditions were then compared to control animals with the aim of identifying unique cellular signatures related to the ischemic response in cells and their spatio-temporal variation.

Material and methods

Experiment design and ischemia mouse model

In our study, we developed a mouse model of ischemia to investigate the effects of hypoxia on brain cells. Mice were anaesthetized with intraperitoneal tribromoethanol (1.25%) and positioned supine on a surgical table. A midline neck incision was made, followed by dissection to expose the carotid arteries. The common carotid artery (CCA), external carotid artery (ECA), and internal carotid artery (ICA) were isolated. The ECA was ligated, and a suture was passed beneath its proximal end. Microvascular clamps occluded the CCA and ICA, and an MCAO thread was inserted via an incision in the ECA into the CCA and then redirected into the ICA. The thread plug was advanced 2 cm into the ICA to induce ischemia for either 30 min or 1 h. After the ischemic period, the thread was withdrawn, the ECA was ligated, and the incision was sutured. Mice were allowed to recover and were returned to their housing cages. We used triplicate models for each experiment (n = 3) and the ischemia group for 30 min was labelled T_30, while the 1-hour ischemia group was labelled T_60. A sham group of animals (n = 3) which underwent the anaesthesia and sham surgery without the introduction of the thread-plug was labelled and used as an experimental control. The cerebral cortex of animals was excised and prepared for separation of nuclei, which was followed by library construction and detailed analysis of the single-cell transcriptome (Figure 1).

Gexscope nuclear separation and quality analysis

The extraction of nuclei from the tissue was performed to prepare RNA libraries and hence high-quality nuclear separation was warranted. Initially, the frozen tissue samples weighing 100 mg were extracted and to eliminate blood stains or

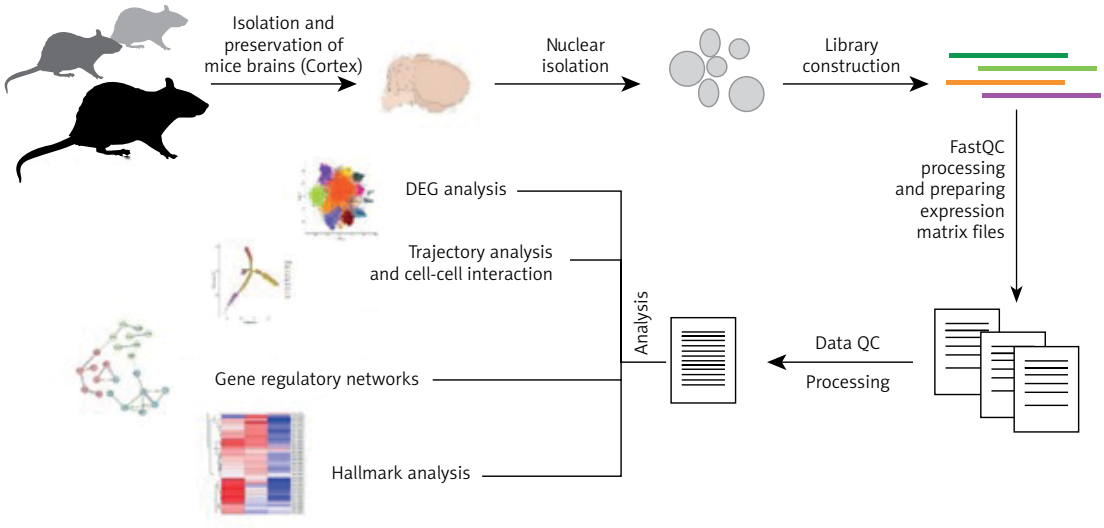

Figure 1. General outline and illustrated methodology of single cell sequencing based analysis of samples. Mouse model of hypoxia was developed using thread-plug method. A group of control mice (dark black), and T_30 (grey) with 30 min hypoxia and T_60 (light grey) were used as experimental groups. The nuclear isolation from excised cerebral cortex and library construction preceded the spatio-temporal analysis of cortical cells. Multi-facet data analysis involved DEG analysis, trajectory analysis, analysis of gene regulatory networks and hallmark analysis

any surface impurities, washing with a pre-cooled PBSE solution (PBS buffer containing 2 mM EGTA) was performed on a temperature-controlled shaker. The tissue was minced using surgical scissors into small pieces. We then used live Tissue Dissociation Solution (Singleron Biotechnologies, cat #1190062) at 37°C for 15 min in a 15 ml centrifuge tube for lysis. The process of lysis was monitored using a light microscope in real time. The resulting mixture was then filtered into a 50 ml centrifuge tube, and subsequent filter screens were washed with a pre-cooled nuclear washing solution. Following centrifugation at 200 relative centrifugal force (RCF) for 2 min, the supernatant was collected.

To monitor the presence of nuclei in the solution we used the DAPI staining procedure followed by routine microscopy. DAPI staining solution (200 µl) was added to the supernatant, followed by the incorporation of 5 ml of pre-cooled PBSE and visualized under a microscope for the nucleic quality check and count. The nuclear solution was filtered using a 40 µm filter and collected nuclei were resuspended in 100-200 µl of pre-cooled PBS, adjusting the nucleus concentration to 3–4 × 10^5 nuclei/ml. Following this, 50 µl of pre-cooled Nuclear Extraction Buffer (NEB) was enriched with RNase inhibitor and DTT at final concentrations of 0.2 U/µl and 1 mM, respectively, and stored for further use.

Single-cell RNA-seq and library preparation

Single-cell nucleus suspensions prepared using Gexscope instructions (as per the previous section) were loaded onto microfluidic devices and used to construct scRNA-seq libraries utilizing the GEXSCOPE Single-Cell RNA Library Kit (Singleron Biotechnologies, #4 161 031) according to the manufacturer's instructions. Briefly, it involved cell lysis, mRNA trapping, labelling cells (barcode), and mRNA (UMI), reverse transcription of mRNA into cDNA, amplification, and eventual fragmentation of cDNA. The individual libraries were diluted to 4 nM and then combined for sequencing on an Illumina HiSeq X, employing 150 bp paired-end reads. In order to ensure data quality, raw reads underwent processing through fastQC and fastp to eliminate low-quality reads. Subsequently, cut-adapt was employed to remove poly-A tails and adaptor sequences. After rigorous quality control measures, the reads were mapped to the reference genome using STAR. Gene counts and UMI counts were obtained through featureCounts software. Expression matrix files, crucial for subsequent analyses, were generated based on these gene counts and UMI counts.

Processing of raw-read data

The initial processing step involved the transformation of raw reads from scRNA-seq into gene expression matrices through an internal pipeline. This sequence began by subjecting the raw reads to quality control using fastQC [18] v0.11.4 (https://www.bioinformatics.babraham.ac.uk/projects/fastqc/) and fastp [19] to eliminate low-quality reads. Subsequent steps included using cutadapt [20] to trim poly-A tails and adapter sequences, followed by extraction of the cell barcode and UMI. For read mapping, STAR [21] v2.5.3a was employed, aligning the reads to the reference genome GRCh38 (ensembl version 92 annotation). UMI counts and gene counts per cell were obtained using featureCounts [22] v1.6.2 software. These counts played a crucial role in generating expression matrix files and facilitating subsequent analyses.

Quality control, dimension reduction and clustering

Before analysis, cells underwent filtration based on specific criteria, including gene counts greater than 100, the top 2% of gene count values, the top 2% of UMI counts, and mitochondrial content exceeding 50%. Following this filtration process, Seurat v2.3 functions were employed for dimension reduction and clustering. Subsequently, normalization and scaling of all genes' expression were executed using the Normalize Data and Scale Data functions. The top 2000 variable genes were selected utilizing the FindVariableFeatures function for principal component analysis (PCA). Employing the top 20 principal components, cells were segregated into distinct clusters through the FindClusters function. Batch effects across samples were mitigated using the Harmony method [23]. Finally, the UMAP algorithm was implemented to visualize cells in a two-dimensional space.

Differentially expressed gene analysis

To identify differentially expressed genes (DEGs), the Seurat FindMarkers function, utilizing the Wilcox likelihood-ratio test and default parameters, was employed. DEGs were defined as genes expressed in more than 10% of cells within a cluster, with an average log (fold change) value exceeding 0.25. For cell type annotation within each cluster, a combination of canonical markers found among the DEGs and insights from the literature was utilized. Visualization of cell type marker expression was accomplished through heatmaps, dot plots, and violin plots generated using Seurat's DoHeatmap, DotPlot, and Vlnplot functions. Doublet cells, characterized by the expression of markers for distinct cell types, were

manually identified and subsequently removed from the analysis.

Pathway enrichment and gene regulatory network inference

To investigate the potential functions of the identified DEGs, Gene Ontology (GO) and Kyoto Encyclopedia of Genes and Genomes (KEGG) analyses were conducted using the "clusterProfiler" R package [24]. Pathways with a p_adj value below 0.05 were considered significantly enriched. Gene Ontology gene sets, covering molecular function (MF), biological process (BP), and cellular component (CC) categories, served as the reference for analysis. Furthermore, predictions regarding protein-protein interactions (PPI) among DEGs within each cluster were made by leveraging known gene interactions linked to relevant GO terms within the StringDB v1.22.0 database.

Gene regulatory network inference

To explore the functions of identified DEGs, we conducted Gene Ontology (GO) and Kyoto Encyclopedia of Genes and Genomes (KEGG) analyses using the "clusterProfiler" R package [24], considering pathways significantly enriched with a p_adj value < 0.05. GO gene sets encompassing molecular function (MF), biological process (BP), and cellular component (CC) categories served as the reference. Protein-protein interaction (PPI) predictions among DEGs within clusters utilized known gene interactions from the StringDB v1.22.0 database. For transcription factor regulatory network analysis, we employed the SCENIC R toolkit [25], integrating scRNA expression matrix and transcription factors from AnimalTFDB, predicting networks with the GENIE3 package based on co-expression patterns. Additionally, we identified transcription factor binding motifs with the RcisTarget package. Defining genes within predicted networks as a gene set, their activity was assessed using the AUCell package to calculate the area under the curve (AUC) value as an indicator of regulatory network activity.

Trajectory and cell-cell interaction analysis

The Monocle2 tool [26] was employed to reconstruct cell differentiation trajectories, ordering cells based on spatial-temporal differentiation using differentially expressed genes. Dimension reduction was performed using DDRTree through FindVariableFeatures. The trajectory was visualized using the plot_cell_trajectory function. Cell-cell interaction analysis utilized CellPhoneDB [27], focusing on receptor-ligand interactions between different cell types or subtypes. To calculate the null distribution of average ligand-receptor expression levels among interacting clusters, 1000 random permutations of cluster labels were performed. The ligand or receptor expression levels were normalized based on the average log gene expression distribution across all cell types using a cutoff value. Significant interactions were identified based on criteria where the *p*-value was < 0.05 and the average log expression exceeded 0.1. Visualization of significant interactions was conducted using the circlize (0.4.10) tool in the R package.

Network analysis

The network of interacting genes was established utilizing the STRING database with the provided input feature. Subsequently, a suitable layout was selected, and gene clustering was performed using the K-means approach. The resulting network maps were exported and employed for further corroboration. Furthermore, Cytoscape was also used for improved visualization of the networks obtained from the STRING database.

Results

Mouse brain cells showed heterogenicity and differential changes in population size after ischemia

The initial challenge after obtaining the single cell data was to cluster the cell types based on their pattern of gene expression. We performed cluster analysis utilizing the Uniform Manifold Approximation and Projection (UMAP) approach, renowned for its robustness, and non-linear dimension reduction. The analysis revealed 12 distinct subpopulations, with neurons predominating alongside oligodendrocytes, astrocytes, microglia, and fibroblasts (Figure 2 A). Regarding cellular origin, the population exhibited a mixture but primarily mirrored the T_60 origin, indicating the predominant cell type. However, cells from other origins closely resembled those from the T_60 experimental group (Figure 2 B). Due to heterogeneity in the expression pattern of neuron-specific markers, neuronal cells were further classified into eight separate sub-populations labelled N1 to N8. Given that neurons constitute the main proportion of each sample and are significantly affected by cerebral ischemia, subsequent analyses were focused on these cells. Fractions of cells among various populations were analyzed and compared between the experimental groups. N1 and N4 populations exhibited a declining trend during ischemia. N1 comprised 0.4% of total cells in the control group, whereas in both ischemic groups (T_30 and T_60), the fractions notably decreased to 0.33%. Similarly, N4 showed proportions of 0.1%, 0.07%, and 0.09% in the control,

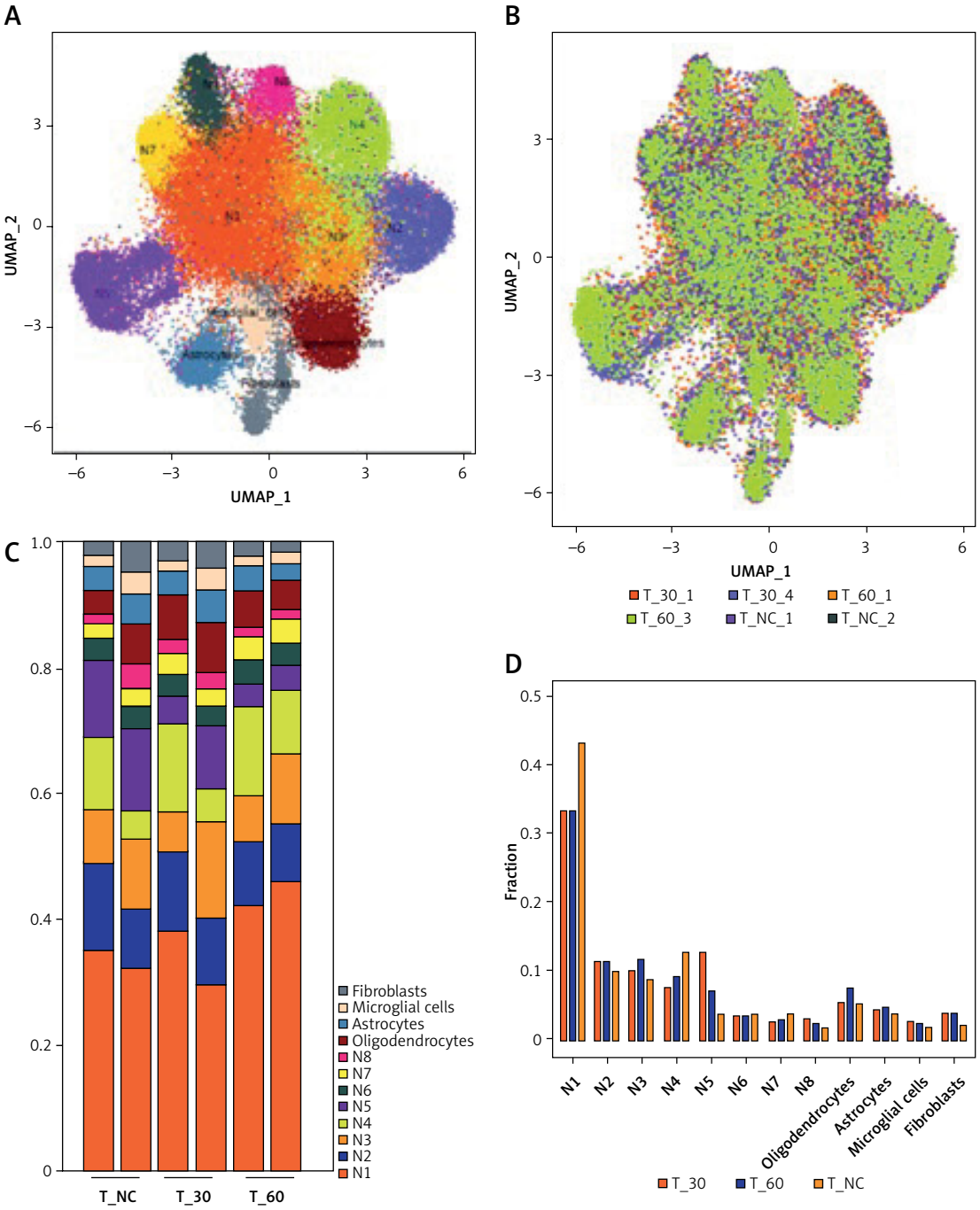

Figure 2. Mouse brain heterogenicity and differential populations as shown by cluster analysis using Manifold Approximation and Projection (UMAP) approach. **A** – Identification of 12 different sub-populations among which predominant cell types were neurons. **B** – Clustering of population types as per their origin. **C** – Relative proportion of cells of various cell types in each experimental group. **D** – Comparative histograms of fractions of each cell type for three experimental groups

T_30, and T_60 groups, respectively. N7, although a minor cell group, exhibited a similar pattern. Another group of cells, including N3 (0.08%, 0.1%, and 0.11%), oligodendrocytes (0.05%, 0.05%, and 0.07%), and astrocytes, demonstrated the highest proportion in T_60 cells, indicating the continuum of cells most affected by ischemia. N2, N8, fibroblasts, and microglial cells responded to ischemia, with proportions significantly higher in the ischemic group compared to the control, yet the difference between the two ischemic groups (T_30 and T_60) was nonsignificant ($p > 0.01$). Interestingly, the N5 population exhibited a unique pattern, with a significantly higher proportion in the T_30 group (0.13%) compared to the control group (0.03%). However, the proportion was restored to 0.07% in the T_60 group. The N6 population of neuronal cells showed no significant differences among the

three experimental groups, suggesting a degree of resilience towards ischemia (Figures 2 C, D). These results are limited by a number of additional factors such as ischemia-induced discomfort to the animal and induced stress, which might not represent actual ischemia in higher organisms.

Post-ischemic differential gene expression suggests changes in cognition and memory

After conducting cell population analysis, our focus shifted to understanding the potential causes of cell dynamics and their impact on various physiological aspects through the Gene Ontology evaluation of differentially expressed genes, including various microRNAs and coding RNAs, specifically in neuronal cells. While gene expression for non-neuronal cell types (oligodendrocytes, astrocytes, and glial cells) was also evaluated, it was not directly relevant to the present hypothesis (see Supplementary material). Our conclusions were derived from three types of pairwise comparisons. In the initial comparison between the control (T-NC) and the 30-minute ischemia group (T_30), we observed significant differences in the expression of 281 transcripts. Filtering out transcripts based on relevance and expression patterns, we selected 40 for further analysis. Gene ontology analysis revealed significant correlations with the top three biological processes – learning and memory, regulation of cell projection organization, and cognition – indicating clinically relevant physiological indicators. The cellular components primarily involved axons and growth cones, with GTPase binding emerging as the primary cellular function impacted during the 30-minute ischemia (Figure 3 A). In the subsequent comparison between the control group and the cortex subjected to 60 min of ischemia (T_60), we identified 472 differentially expressed transcripts. After filtering out non-significant or non-relevant genes, Gene Ontology analysis indicated similarities with the T_30 group, with cognition and learning as top processes, and an additional impact on locomotory behavior observed. Contrary to the T_30 group, the T_60 group exhibited differences in both molecular signaling and cellular locations of differentially expressed proteins, with most proteins localized in the cell's leading edge or post-synaptic area (Figure 3 B). In the third comparison between the cortex subjected to 30 min of ischemia (T_30) and 60 min of ischemia (T_60), we identified 177 differentially expressed transcripts. After excluding non-significant genes, Gene Ontology analysis revealed cognition as a significant biological process, with the synaptic vesicle cycle and vesicle-mediated transport emerging as highly significant processes in this comparison. This finding was supported by cellular compartment ontology. Additionally, calmodulin and calcium-mediated signaling were implicated in driving prolonged changes due to ischemia, indicating their potential role in mediating ischemic effects (Figure 3 C). The gene expression patterns in higher organisms are also a subject of various secondary factors such as additional epigenetic regulation and stress-induced post-translational modification of proteins, which could not be assessed in the present study.

Furthermore, the network and interaction analysis of translational products of active transcripts resulted in a closely interacting network of more than 20 proteins organized into three distinct clusters (K-means), suggesting possible cross talk and a potential role of these biological interactions pertaining to ischemic insult.

Post-ischemic differential gene expression is associated with enhanced cell-cell interaction and temporal changes in cell differentiation

To explore the potential underlying cellular mechanisms driving the observed changes in expression patterns across experimental groups, we conducted microenvironment cell-interaction analysis and trajectory analysis of neuronal cell subpopulations. Trajectory analysis involved examining gene expression profiles from individual cells to reconstruct developmental or differentiation paths. Starting with single-cell RNA sequencing data, we implemented preprocessing steps, including quality control and clustering to group cells with similar expression profiles. The core of trajectory analysis lies in reconstructing cellular paths using algorithms that order cells along a continuum (pseudotime) or model transitions between cell states. Visualization tools aided in reconstructing paths as lineage trees or plots, facilitating an understanding of cellular relationships. The cell interaction analysis revealed that in the cerebral ischemia model, the overall interaction between cells significantly increased after 30 min of treatment, surpassing even the 60-minute mark. Fibroblast-neuron cell interactions showed progressive enhancement during the disease and may be associated with disease progression. While neuron-neuron interactions were predominant in the control group, there was a significant increase in neuron-astrocyte and neuron-fibroblast interactions in the T_30 population. Moreover, in the T_60 group, neuron-fibroblast interaction appeared stronger and dominant compared to neuron-astrocyte interaction, which was more prominent in the T_30 population (Figure 4 A). As a limitation, it must be admitted that time points T_30 and T_60 lie somewhere in between the ischemia-mediated adaptability and beginning of changes, yet there may be some initial stimulus

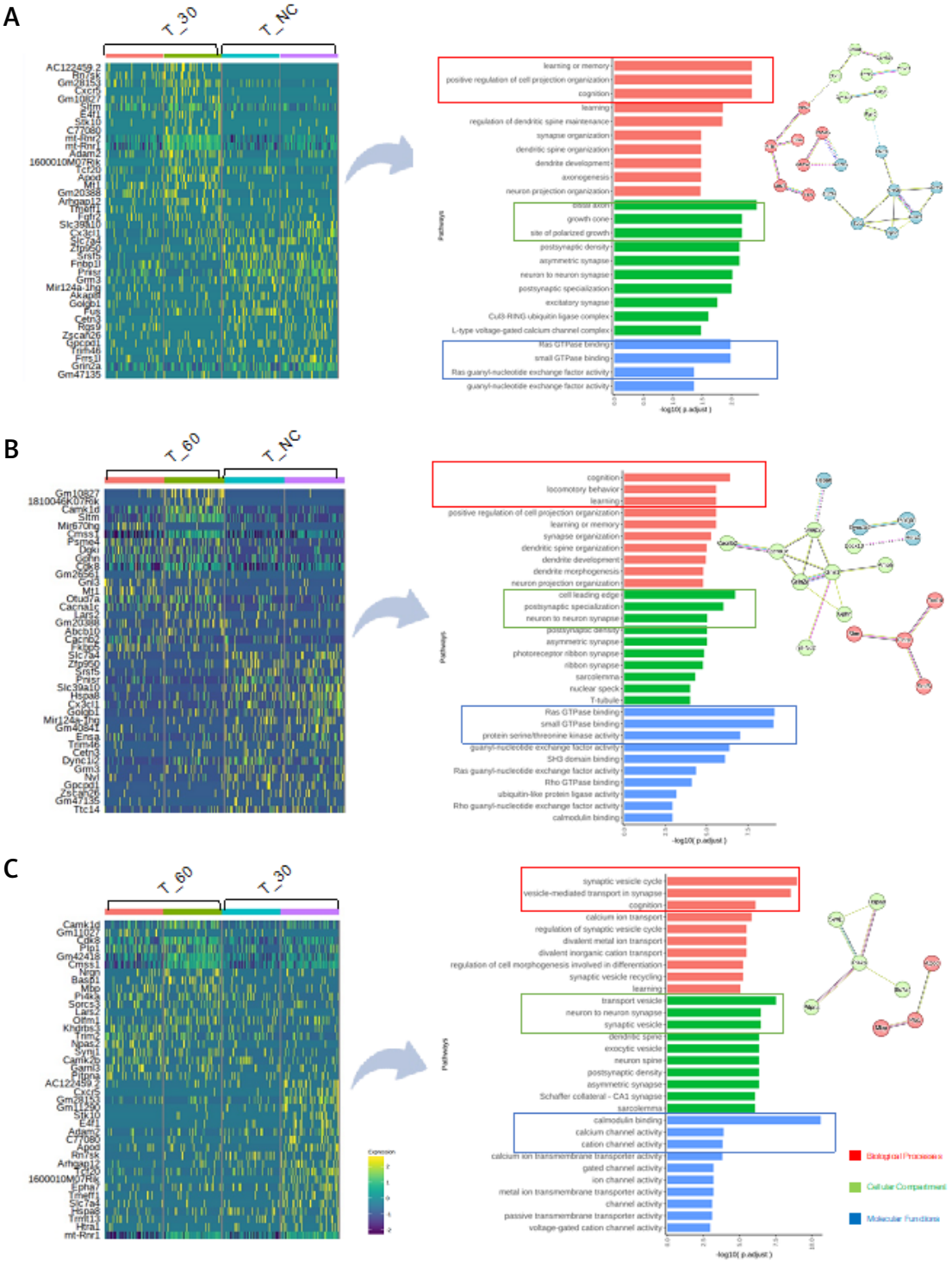

Figure 3. Gene expression profiles (heatmaps) and Gene Ontology analysis reveals the key networks which differ between experimental conditions. **A** – T_30 vs control group. **B** – T_60 vs control group. **C** – T_30 vs T _60. Gene Clusters in T_30 vs control: Cluster 1 included genes such as Abcb10, Akap8l, C77080, Cetn3, Cmss1, E4f1, Fus, Gm20388, Htra1, Mef2c, Mnat1, Mt1, Phactr1, Pnisr, R3hdm1, Sltm, Srsf5, Tcf20, Tmeff1, Trim46, Trpm3, Vxn, Zfp950, Zscan26, mt-Co1, mt-Nd5. Cluster 2 contained genes such as Adam2, Apod, Atp2b1, Calm1, Camk1d, Chn1, Cx3cl1, Cxcr5, Dync1i2, Ensa, Fgfr2, Fnbp1l, Golgb1, Gpcpd1, Kazn, Rere, Slc39a10, Slc7a4, Sorl1, and Stk10. Cluster 3 included genes such as Arhgap12, Atp2b2, Dock10, Frrs1l, Gphn, Gpm6b, Grin2a, Grin2b, Grm3, Hsph1, Nell2, Plcb1, Snhg11, Syt1, mt-Nd2. Gene Clusters in T_60 vs control group: Cluster 1 (Gnl3, Pnisr, Sltm, Snhg11, Srsf5, Ttc14 – highlighted in red). Cluster 2 (Amph, Cacna1c, Cacnb2, Camk1d, Cdk8, Cmss1, Cx3cl1, Dgki, Dock10, Ensa, Gm20388, Gphn, Grin1, Grin2a, Mt1, Otud7a, Slc39a10, Snap25, Trim2, Zfp950, mt-Nd2 – highlighted in green). Cluster 3 (1810046K07Rik, Dync1i2, Golgb1, Herc1, Hspa8, Psme4, Slc7a4). Gene Clusters in T_30 vs T_60 Group: Cluster 1 (Apod, Mbp, Plp1 – highlighted in red) and Cluster 2 (Hspa8, Pi4ka, Pitpna, Slc7a4, and Synj1), suggesting possible post-translational cross-talk

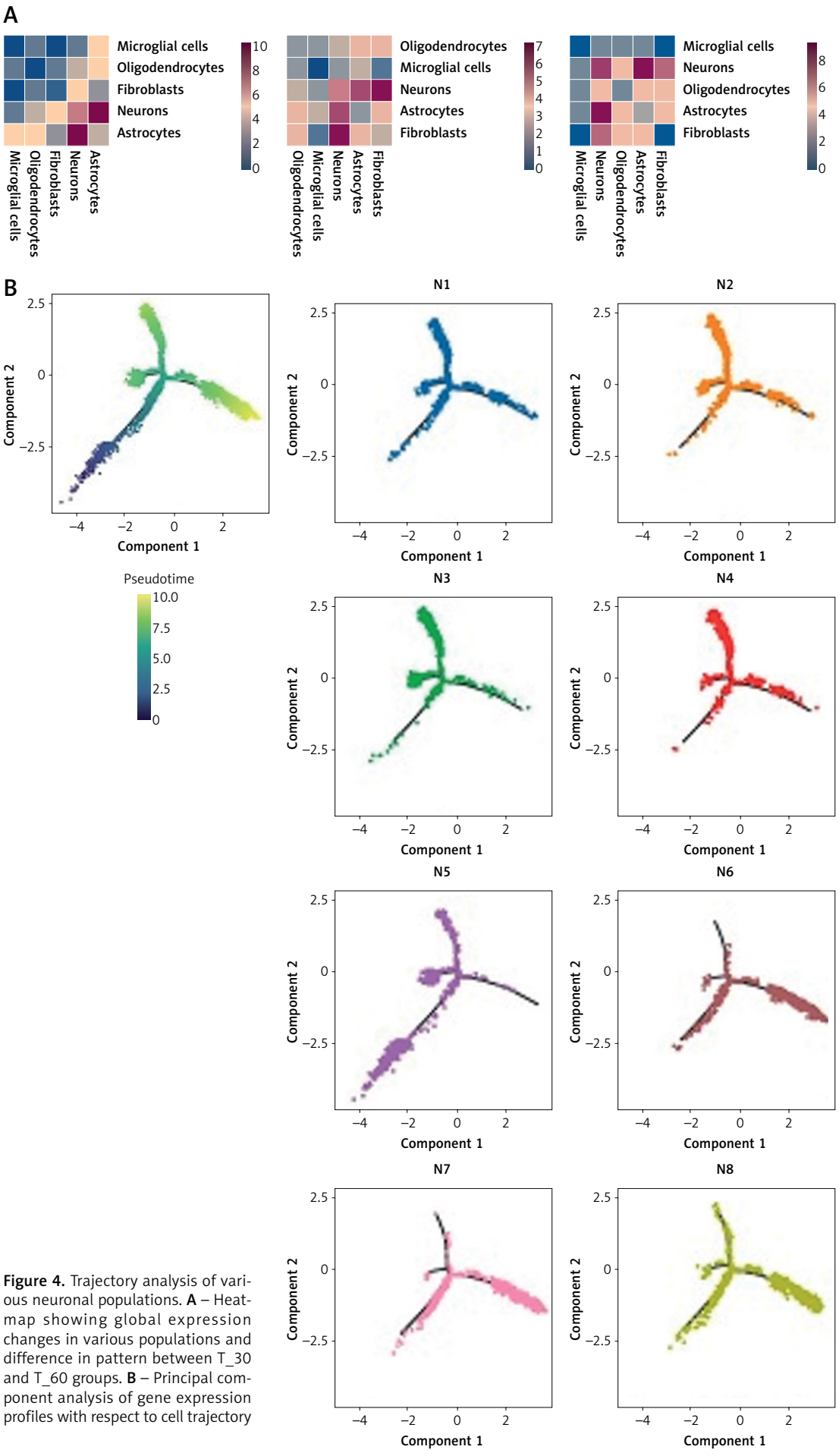

Figure 4. Trajectory analysis of various neuronal populations. **A** – Heatmap showing global expression changes in various populations and difference in pattern between T_30 and T_60 groups. **B** – Principal component analysis of gene expression profiles with respect to cell trajectory

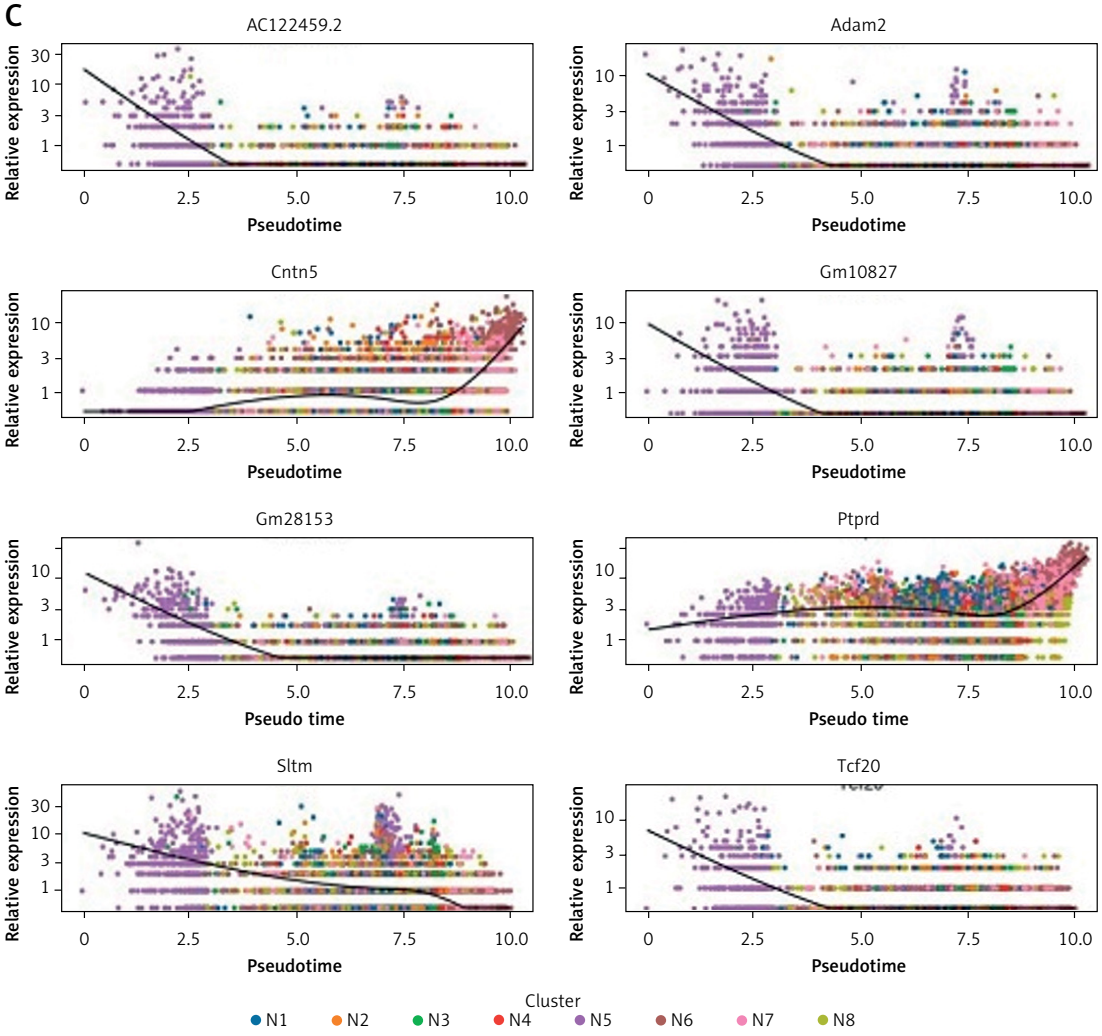

Figure 4. Cont. **C** – Analysis of gene expression profiles of selected genes for various neuronal populations (N1 to N8)

caused by ischemia, possibly induced by radicals and PTMs, which are discussed elsewhere in previous studies and thus are not the focus of the current study.

During PCA, we observed variations in expression patterns among populations. While populations N1, N2, N3, and N8 were homogeneous across the two components, population N5 displayed high heterogeneity and an inclination towards component 1 (Figure 4 B). Furthermore, the differential dot plots of selected genes across all neural populations refined the expression profiles, indicating that the N5 population of neurons showed significantly higher upward expression of genes Adam2, Gm10827, Ptprd, Sltm, Cntn5, and AC122450.2. Genes Gm28153 and Tcf20 exhibited increased expression in N8 and N6 populations (Figure 4 C), while all other populations were heterogeneous for the aforementioned gene expression, providing intriguing mechanistic insights into the trajectory of N5 cells.

Angiogenesis, hypoxia and proliferation are the most affected cellular-physiological indices in the ischemic cortex

To draw conclusive insights from the single-cell genomics dataset, we conducted hallmark analysis and further investigated genes associated with key processes. Gene set variation analysis (GSVA) of the HALLMARK dataset revealed significant differences in gene sets across various stages, encompassing angiogenesis, hypoxia, proliferation, and other pathways significantly enriched during ischemia. However, functions such as oxidative phosphorylation and pancreatic β cells exhibited significant weakening (Figure 5 A). The differential expression of hypoxia, angiogenesis, and proliferation-related gene sets in the three groups of sample neurons showed notable distinctions, particularly between the T_30 and T_60 groups in comparison to the control. As the model treatment time extended, substantial differences emerged in the

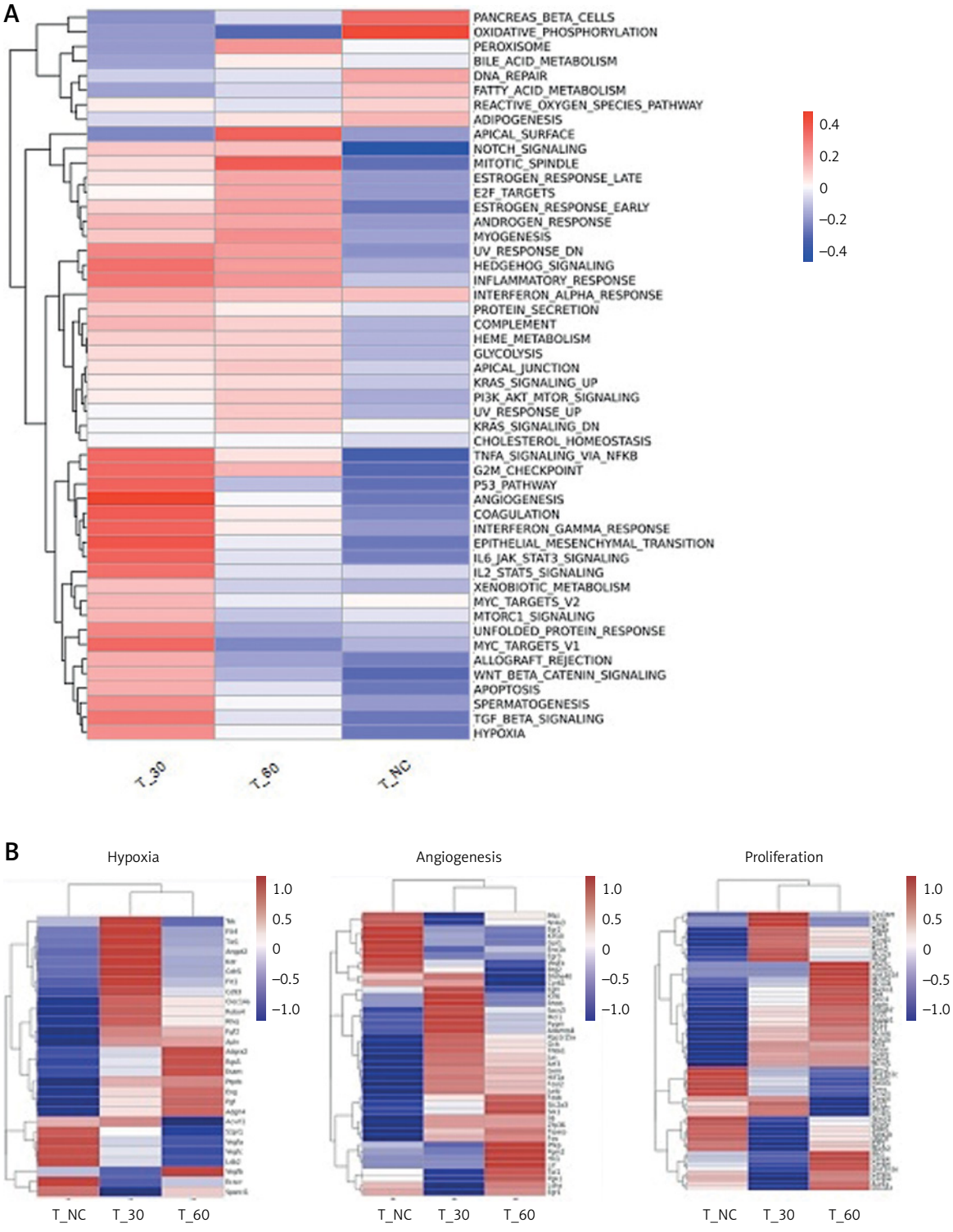

Figure 5. Hallmark analysis and overview of the hallmarks. **A** – Heatmap indicating key processes identified in experimental groups based on hierarchical clustering. **B** – Elaborated heat maps of hypoxia, angiogenesis and proliferation specific genes differentially expressed in three experimental groups

expression patterns of various genes (Figure 5 B). The hallmark analysis is still subject to correlation with other genetic and lifestyle-induced changes in the brain; hence to establish these hallmarks as an exclusive conclusion in our experimental model is still a challenge which must be explored further in future studies.

Discussion

In humans, prolonged oxygen deprivation induces pulmonary arterial hypertension (PAH). Traditionally, researchers employ rodent models exposed to hypoxia to study this condition [28]. With the advent of single-cell RNA sequencing, we can now explore hypoxia-induced changes in gene activity at a cell-specific level in live organisms [29, 30]. Previous studies using a mouse model of hypoxia identified that hypoxia influences the quantities of specific cell types, particularly immune and endothelial cells in the lung. It was indicated in several studies that hypoxia preconditioning for 180 min and above results in relative hypoxic tolerance, but the induction of genes by hypoxia is apparent in the 30–60-min period [31, 32]. Hence, we chose two typical conditions of hypoxia exposure, T_30 and T_60, to understand well the temporal switching of hypoxia-inducible genes. They investigated the role of Notch 3 genes by employing single-cell RNA sequencing to compare lung cells of wild-type (Wt) mice exposed to 28 days of hypoxia against those of control mice in normoxic conditions [33]. Additionally, hypoxia, a hallmark of cancers, was examined using single-cell sequencing in a study by Yanru Zhang. The study revealed significant interactions, particularly between macrophages and tumor cells, in this oxygen-deprived microenvironment. We also observed distinctive functional variations among tumor cells, identifying a subset under hypoxia displaying remarkably high invasive potential. By constructing gene regulatory networks specific to cell conditions, we pinpointed several controllers that respond to a hypoxic microenvironment such as the Ras-mediated pathway, calmodulin and calcium-mediated signaling, etc. Finally, we validated that reducing the expression of two pivotal controllers, CEBPD and FOSL1, diminished the invasive capacity of glioblastoma multiforme (GBM) cells during hypoxia [30]. Recent research aimed to identify potential therapeutic targets to support cell survival in the mouse brain penumbra, employing not only single-cell sequencing but also a combinatorial approach with bulk RNA-seq analysis [34]. Through single-cell sequencing of the mouse cortex at 12 h and 24 h after transient middle cerebral artery occlusion (tMCAO), the authors detected dynamic changes in astrocytes during acute ischemic stroke. Furthermore, they identified three major astrocyte subtypes at each time point, revealing significant differences in gene expression and metabolic pathways, particularly highlighting a major shift in energy metabolism [35]. Our study represents an advancement in understanding the neuronal response and heterogeneity of cell-level gene expression during acute hypoxia, addressing temporal differences in expression and cellular profiles in the cortex regions of the brain. Employing single-cell genomics and Uniform Manifold Approximation and Projection (UMAP) for cluster analysis, we identified 12 distinct subpopulations, primarily neurons, alongside oligodendrocytes, astrocytes, microglia, and fibroblasts, during 60 min of hypoxic conditions.

The unique ability of the N6 population to show resilience towards ischemia was noteworthy and remains a subject of further exploration. To investigate the underlying mechanisms, microenvironment cell-interaction analysis revealed enhanced interactions after 30-minute ischemia, particularly fibroblast-neuron interactions, potentially linked to disease progression. Trajectory analysis reconstructed cell paths, showing varied cellular relationships and heterogeneity, especially in N5. Differential dot plots highlighted distinct gene expression in different neuronal populations, suggesting potential mechanistic insights into the N5 trajectory. Additionally, PCA illustrated expression pattern differences among populations, particularly emphasizing the heterogeneity of N5 inclined towards a specific component. Notably, certain genes showed pronounced expression changes in specific neuronal populations, indicating potential involvement in the trajectory of N5 cells. Furthermore, the unique feature of the study was the application of Gene Ontology to unravel the underlying mechanisms impacting various physiological aspects, focusing primarily on differentially expressed microRNAs and coding RNAs in neuronal cells. We deciphered unique pathways associated with 30-minute and 60-minute hypoxia, establishing the contrast and shift in the metabolic cascades.

To delineate gene expression differences between experimental groups, three pairwise comparisons were conducted. In the first comparison between the control and 30-minute ischemia groups (T_30), we identified 281 differentially expressed transcripts. Subsequent Gene Ontology analysis highlighted significant correlations with biological processes related to learning and memory, cell projection organization regulation, and cognition. Additionally, cellular components implicated axons and growth cones, with GTPase binding as a key affected cellular function during the 30-minute ischemia period. The second comparison, comparing the control and 60-minute ischemia cortex (T_60), identified 472 differentially

expressed transcripts. Remarkably, the biological processes affected in T_30 were retained, with the addition of locomotory behavior impact. Network analysis uncovered distinct interaction patterns among RNA-mapped proteins, again grouped into three clusters, suggesting potential post-translational crosstalk. In the third comparison, between T_30 and T_60, 177 differentially expressed transcripts were identified. Notably, cognitive processes persisted, with the synaptic vesicle cycle and vesicle-mediated transport emerging as significant biological processes in this prolonged ischemia context. Molecular function analysis highlighted the involvement of calmodulin and calcium-mediated signaling. Network analysis again delineated three distinct hubs of interacting proteins, hinting at potential post-translational regulatory pathways.

Notably, T_30 and T_60 samples, which varied in their hypoxic exposure, exhibited distinct sets of regulatory mechanisms. In T_30, hypoxia-responsive genes primarily included Tek, Fit4, Tie1, Anggt 2, Kdr, Cdh5, Fit1, Cd93, Clec149, Robo4, Rhoi, Fgf2, and Apin. The expression of these genes in hypoxia is line with previous findings, suggesting the transformation of a subset of glioblastoma stem-like cells (GSCs) expressing the endothelial cell marker CDH5, leading to their ability to transdifferentiate into endothelial cells and form blood vessels [36]. Additionally, it is established that hypoxia-induced FGF2 plays a role in both negative and positive feedback interactions with HIF-1alpha at the translational level [37], indicating the activation of a conventional hypoxia-induced feedback loop in a cell-type-specific manner. In contrast, T_60 exhibited a different response, showing the upregulation of a distinct set of hypoxia-responsive genes, which clustered together during our analysis. These genes included Adgra, Rgs5, Esam, Pfprb, Eng, Pgf, and Adgrl4. Previous studies have emphasized that the survival of deep-layer neurons and the formation of the cortex are influenced by hypoxia signaling dependent on Hif1α, and our study provided new evidence on the temporal segregation of cell-type-specific modulation of Hif-induced activation [38].

In this study, we were unable to precisely elucidate the reason behind this observed shift. Additionally, the angiogenic markers identified in T_30-specific neuronal populations – Cyr61, Egfr, Kit6, Rhob, Socs3, Mci1, Pygm, Adsmts4, Ppplr15a, Gck, Thps1, Jun, Atf3, Gem – remained distinctly clustered compared to the T_60 subset of neuronal populations, suggesting the activation of a different cascade in prolonged hypoxia in contrast to the acute response.

The proliferation-specific genes that were upregulated included Ube2c, Foxm1, Hist1h1d, Mcm2, Mcm4, and Nucks1. While the role of the Mcm family of proteins in the hypoxia response is unclear, studies suggest that MCM2, MCM4, and MCM6 markers serve multiple purposes, such as distinguishing between luminal A and luminal B subtypes in breast cancer, exploring their heightened expression in triple-negative breast cancer, and evaluating their prognostic significance in predicting relapse-free survival [39]. Therefore, we propose further exploration of this gene family as a potential hallmark of hypoxic changes in the cortex, emphasizing the need to distinguish between cancer-related pathways and hypoxia-induced pathways.

The outcomes of these comparisons reveal the dynamic shifts in gene expression patterns during various phases of cerebral ischemia. The persistence of cognitive processes across comparisons and the emergence of additional processes, such as locomotory behavior and synaptic vesicle cycling, underscore the progressive impact of ischemia on neuronal function. The identified protein clusters and interaction patterns suggest potential post-translational regulatory mechanisms underpinning these changes. These findings pave the way for further exploration into specific molecular pathways contributing to neuronal responses during ischemia, potentially uncovering novel therapeutic targets or intervention strategies to alleviate ischemic damage in the brain. The study's strength lies in its comprehensive examination of cellular changes in response to cerebral ischemia using cutting-edge single-cell genomic techniques, highlighting the dynamics of specific neuronal subpopulations and interactions between different cell types.

Despite its insightful findings, the study has notable limitations. The ischemic model may not fully replicate human ischemia due to species differences and simplified hypoxic conditions, potentially limiting translational relevance. The study's temporal resolution, examining only two time points, may overlook crucial intermediate responses. Additionally, the technical variability and dropout events inherent in single-cell RNA sequencing can introduce biases, affecting the accuracy and reproducibility of gene expression data. These factors highlight the necessity for further research to address these limitations and enhance our understanding of ischemic mechanisms for developing targeted therapies. Moreover, the model that we used in our study also has limitations regarding stroke attack stability, predictability, infarct sizes, and locations, complicating the translation of findings to clinical applications. The study was also unable to identify some recently explored aspects of molecular insight of ischemia, such as involvement of miRNAs, which is also an active area of ischemia research [40, 41]. Nevertheless, our study provides novel conclusions on the temporal and spatial

heterogenicity of cortical cells in a mouse model of ischemia, which might be implicated in human health in future. However, the direct extrapolation of these findings to humans and primate models is not quite straightforward and remains a complicated research question, which needs to be answered by conducting clinical studies and corroborating the present findings. The primary factors that might lead to discrepancies and affect extrapolation to humans include the lifestyle, diet, and genetic heterogenicity in the human population as compared to the almost homogeneous mouse models used in the present study.

The present study provides insights into spatio-temporal heterogenicity of the neuronal cells in controlled acute ischemia in mice models. It is quite interesting that neuronal cells under ischemia can be broadly segregated into 12 different profiles. Further, dissection of expression profiles and network analysis showed the learning, memory and cell projection organization as the most affected biological process in 30 min of ischemia, while the impact on cognition and locomotory behavior was observed in 60 min of ischemia. Furthermore, our study was also able to delineate the calmodulin and calcium-mediated molecular process as a key switch during the transition from 30-minute to 60-minute ischemia. Nevertheless, additional validation and functional studies are necessary to confirm the implications of these observed cellular changes and interactions in the context of cerebral ischemia.

Acknowledgments

Both Ting Lu and Shengzhen Hou contributed equally to the study.

We are thankful to Dr. Jinping Zhang for critically editing the current manuscript.

Funding

This study was supported by the Shandong Province Medical and Health Science and Technology Project (Project No. 202303071294).

Ethical approval

This study was approved by the Ethical Committee of Affiliated Hospital of Shandong University of Traditional Chinese Medicine (Approval No. AHSU-2023-082).

Conflict of interest

The authors declare no conflict of interest.

References

1. Lusis AJ. Atherosclerosis. Nature 2000; 407: 233-41.
2. Kalogeris T, Baines CP, Krenz M, Korthuis RJ. Cell biology of ischemia/reperfusion injury. Int Rev Cell Mol Biol 2012; 298: 229-317.
3. Price AJ, Wright FL, Green J, et al. Differences in risk factors for 3 types of stroke: UK prospective study and meta-analyses. Neurology 2018; 90: e298-e306.
4. Soler EP, Ruiz VC. Epidemiology and risk factors of cerebral ischemia and ischemic heart diseases: similarities and differences. Curr Cardiol Rev 2010; 6: 138-49.
5. Bonita R. Epidemiology of stroke. Lancet 1992; 339: 342-4.
6. Feigin VL, Lawes CM, Bennett DA, Anderson CS. Stroke epidemiology: a review of population-based studies of incidence, prevalence, and case-fatality in the late 20th century. Lancet Neurol 2003; 2: 43-53.
7. Tu WJ, Zhao Z, Yin P, et al. Estimated burden of stroke in China in 2020. JAMA Netw Open 2023; 6: e231455.
8. Wang W, Jiang B, Sun H, et al. Prevalence, incidence, and mortality of stroke in China: results from a nationwide population-based survey of 480 687 adults. Circulation 2017; 135: 759-71.
9. Rubin MN, Barrett KM. What to do with wake-up stroke. Neurohospitalist 2015; 5: 161-72.
10. Yew KS, Cheng EM. Diagnosis of acute stroke. Am Fam Physician 2015; 91: 528-36.
11. Trivedi JK. Cognitive deficits in psychiatric disorders: current status. Indian J Psychiatry 2006; 48: 10-20.
12. Imran R, Mohamed GA, Nahab F. Acute reperfusion therapies for acute ischemic stroke. J Clin Med 2021; 10: 3677.
13. Okumura E, Tsurukiri J, Ota T, et al. Outcomes of endovascular thrombectomy performed 6-24 h after acute stroke from extracranial internal carotid artery occlusion. Neurol Med Chir (Tokyo) 2019; 59: 337-43.
14. Winnige P, Vysoky R, Dosbaba F, Batalik L. Cardiac rehabilitation and its essential role in the secondary prevention of cardiovascular diseases. World J Clin Cases 2021; 9: 1761-84.
15. Herpich F, Rincon F. Management of acute ischemic stroke. Crit Care Med 2020; 48: 1654-63.
16. Campbell BCV, De Silva DA, Macleod MR, et al. Ischaemic stroke. Nat Rev Dis Primers 2019; 5: 70.
17. Safdieh JE, Govindarajan R, Gelb DJ, Odia Y, Soni M. Core curriculum guidelines for a required clinical neurology experience Neurology 2019; 92: 619-626. Erratum in: Neurology 2019; 93: 135.
18. de Sena Brandine G, Smith AD. Falco: high-speed FastQC emulation for quality control of sequencing data. F1000Res 2019; 8: 1874.
19. Chen S, Zhou Y, Chen Y, Gu J. fastp: an ultra-fast all-in-one FASTQ preprocessor. Bioinformatics 2018; 34: i884-90.
20. Kechin A, Boyarskikh U, Kel A, Filipenko M. cutPrimers: A New Tool for Accurate Cutting of Primers from Reads of Targeted Next Generation Sequencing. J Comput Biol 2017; 24: 1138-43.
21. Dobin A, Davis CA, Schlesinger F, et al. STAR: ultrafast universal RNA-seq aligner. Bioinformatics 2013; 29: 15-21.
22. Liao Y, Smyth GK, Shi W. featureCounts: an efficient general purpose program for assigning sequence reads to genomic features. Bioinformatics 2014; 30: 923-30.
23. Korsunsky I, Millard N, Fan J, et al. Fast, sensitive and accurate integration of single-cell data with Harmony. Nat Methods 2019; 16: 1289-96.
24. Yu G, Wang LG, Han Y, He QY. clusterProfiler: an R package for comparing biological themes among gene clusters. OMICS 2012; 16: 284-7.
25. Aibar S, González-Blas CB, Moerman T, et al. SCENIC: single-cell regulatory network inference and clustering. Nat Methods 2017; 14: 1083-6.

26. Qiu X, Hill A, Packer J, Lin D, Ma YA, Trapnell C. Single-cell mRNA quantification and differential analysis with Census. Nat Methods 2017; 14: 309-15.
27. Efremova M, Vento-Tormo M, Teichmann SA, Vento-Tormo R. CellPhoneDB: inferring cell-cell communication from combined expression of multi-subunit ligand-receptor complexes. Nat Protoc 2020; 15: 1484-506.
28. Porteous MK, Fritz JS. Hypoxemia in a patient with pulmonary arterial hypertension: getting to the heart of the matter. Ann Am Thorac Soc 2014; 11: 836-40.
29. Tang F, Barbacioru C, Wang Y, et al. mRNA-Seq whole-transcriptome analysis of a single cell. Nat Methods 2009; 6: 377-82.
30. Zhang Y, Zhang B, Lv C, et al. Single-cell RNA sequencing identifies critical transcription factors of tumor cell invasion induced by hypoxia microenvironment in glioblastoma. Theranostics 2023; 13: 3744-60.
31. Prass K, Scharff A, Ruscher K, et al. Hypoxia-induced stroke tolerance in the mouse is mediated by erythropoietin. Stroke 2003; 34: 1981-6.
32. Fluri F, Schuhmann MK, Kleinschnitz C. Animal models of ischemic stroke and their application in clinical research. Drug Des Devel Ther 2015; 9: 3445-54.
33. Thomas S, Manivannan S, Garg V, Lilly B. Single-cell RNA sequencing reveals novel genes regulated by hypoxia in the lung vasculature. J Vasc Res 2022; 59: 163-75.
34. Guo K, Luo J, Feng D, et al. Single-cell RNA sequencing with combined use of bulk RNA sequencing to reveal cell heterogeneity and molecular changes at acute stage of ischemic stroke in mouse cortex penumbra area. Front Cell Dev Biol 2021; 9: 624711.
35. Ma H, Zhou Y, Li Z, et al. Single-cell RNA-sequencing analyses revealed heterogeneity and dynamic changes of metabolic pathways in astrocytes at the acute phase of ischemic stroke. Oxid Med Cell Longev 2022; 2022: 1817721.
36. Mao XG, Xue XY, Wang L, et al. CDH5 is specifically activated in glioblastoma stemlike cells and contributes to vasculogenic mimicry induced by hypoxia. Neuro Oncol 2013; 15: 865-79.
37. Conte C, Riant E, Toutain C, et al. FGF2 translationally induced by hypoxia is involved in negative and positive feedback loops with HIF-1alpha. PLoS One 2008; 3: e3078.
38. Sakai D, Sugawara T, Kurokawa T, et al. Hif1α dependent hypoxia signaling contributes to the survival of deep-layer neurons and cortex formation in a mouse model. Mol Brain 2022; 15: 28.
39. Issac MSM, Yousef E, Tahir MR, Gaboury LA. MCM2, MCM4, and MCM6 in breast cancer: clinical utility in diagnosis and prognosis. Neoplasia 2019; 21: 1015-35.
40. Zhu S, Tang J, Lan L, Su F. Inhibition of miR-34a ameliorates cerebral ischemia/reperfusion injury by targeting brain-derived neurotrophic factor. Arch Med Sci 2021. doi: 10.5114/aoms/143303.
41. Duan Q, Sun W, Yuan H, Mu X. MicroRNA-135b-5p prevents oxygen-glucose deprivation and reoxygenation-induced neuronal injury through regulation of the GSK-3α/Nrf2/ARE signaling pathway. Arch Med Sci 2018; 14: 735-44.